LAWRENCE
LIVERMORE
NATIONAL
LABORATORY

UCRL-JRNL-226102

Photon Production through Multi-step Processes Important in Nuclear Fluorescence Experiments

C. Hagmann, J. Pruet

November 14, 2006

Nuclear Instruments and Methods B

Photon Production through Multi-step Processes Important in Nuclear Resonance Fluorescence Experiments

C. Hagmann & J. Pruet

Lawrence Livermore National Laboratory, 7000 E. Ave, Livermore, CA

Abstract

We present calculations describing the production of photons through multi-step processes occurring when a beam of gamma rays interacts with a macroscopic material. These processes involve the creation of energetic electrons through Compton scattering, photo-absorption and pair production, the subsequent scattering of these electrons, and the creation of energetic photons occurring as these electrons are slowed through Bremsstrahlung emission. Unlike single Compton collisions, during which an energetic photon that is scattered through a large angle loses most of its energy, these multi-step processes result in a sizable flux of energetic photons traveling at large angles relative to an incident photon beam. These multi-step processes are also a key background in experiments that measure nuclear resonance fluorescence by shining photons on a thin foil and observing the spectrum of back-scattered photons. Effective cross sections describing the production of backscattered photons are presented in a tabular form that allows simple estimates of backgrounds expected in a variety of experiments. Incident photons with energies between 0.5 MeV and 8 MeV are considered. These calculations of effective cross sections may be useful for those designing NRF experiments or systems that detect specific isotopes in well-shielded environments through observation of resonance fluorescence.

Key words: X-ray beams and x-ray optics, X-ray scattering, Photon absorption and scattering
PACS: 41.50.+h, 78.70.Ck, 25.20.Dc

1 INTRODUCTION

Schiff [1] pointed out that multi-step processes rather than discrete photon scatterings would create the principal background in experiments observing nuclear resonance fluorescence (NRF). In these experiments a beam of $\gamma-$rays

is shined on a target, which is usually made of a thin foil. Resonance fluorescence and fine details of nuclear structure are studied by observing photons emitted during the de-excitation of target nuclei that have absorbed incident photons [2]. Multi-step processes refer to interactions in which the transfer of energy carried by incident photons to scattered photons is mediated by an electron traveling in the target material. Since Schiff's early suggestion, dozens of successful (γ, γ') NRF experiments have confirmed the presence of a substantial and relatively complicated background that cannot be explained by single photon scatterings (see [3] for a recent review).

In this paper we present calculations describing production of back-scattered photons through multi-step processes. This effort is analogous to more mature studies of bremsstrahlung production resulting from the collision of energetic electrons with a target [4]. There are two important differences though. One is just that here the incident beam is made up of photons rather than electrons. The other is more practical and relates to intended application. Studies of light production with electron beams are usually concerned with the spectrum and power of the light source. For this reason most emphasis is on the conversion efficiency for radiation emitted in the forward direction, or direction of the incident electron beam. By contrast, NRF experiments typically observe back-scattered radiation so as to avoid backgrounds from Compton interactions in the target material. The importance of these backgrounds is determined by their strength relative to the cross sections characterizing resonant absorption and other sources of background. For these reasons the present paper concentrates on production of radiation emitted at large angles relative to an incident beam. Results are presented in terms of "effective cross sections", which are related in a simple way to efficiency for photon production. Though our definition of effective cross sections represents some abuse of a well established convention, it is useful for allowing simple comparisons against microscopic processes whose cross sections are well known.

One aim of this paper is to fill a basic data gap that hinders a quantitative understanding of some photon scattering experiments. For the most part all of the single-step microscopic processes that create appreciable backgrounds in NRF experiments have been well studied. These include Compton scattering and a variety of elastic processes like Rayleigh, Nuclear Thomson and Delbrück interactions [5,6]. Interested researchers can find formulas or tables describing these processes in the literature [5,7,8]. By contrast, tables of efficiency or effective cross sections characterizing multi-step processes have not been previously presented. As these interactions can cause the lion's share of background in NRF experiments a compact presentation seems useful.

A second aim of this paper is to elucidate some implications of multi-step processes for experiments. To this end we present estimates of backgrounds expected in experiments that use bremsstrahlung or nearly monochromatic

laser/linac light sources [9,10] to induce and observe NRF. The steeply rising backgrounds from multi-step processes can be a key input to decisions for design of NRF experiments.

2 Basic Considerations

For the sake of presenting some framework and notation for later discussion we give in this section a basic account of well-known processes governing the birth, slowing and bremsstrahlung emission off of energetic electrons. However, this paper does not provide a simple theory or derive equations that describe emission by multi-step processes. We instead rely on Monte Carlo calculations. A simple first principles description of effective cross section for photon production through multi-step processes would be a useful addition to the NRF literature.

In the system we consider a photon is incident normally on a plane slab of material. The amount of material traversed by this photon before interacting is given by

$$\rho L_\gamma = \frac{A}{N_a \sigma^{\rm tot}} \approx 10(A/Z)\,{\rm g/cm^2}. \tag{1}$$

Here ρ is the density of the target material, L_γ is the photon mean free path, A is the mass number of target atoms, N_a is Avogadro's number, and $\sigma^{\rm tot}$ represents the total photon interaction cross section. The number on the right hand side of this equation assumes that Compton scattering dominates the photon interaction. It is good to within about 50% for all elements and for photons with incident energies in the range of 2-4 MeV.

Our interest here is in processes that give rise to energetic back-scattered photons. Compton scattering between an incident photon and an electron in the irradiated target cannot result in the production of an energetic (multi-MeV) backscattered photon because too much energy is given to the electron. However, there are several ways in which the incident photon can give all or almost all of its energy to an electron. Depending on the energy and target material this can occur through Compton scattering, pair production, or photo-electric absorption. To a first approximation the Compton scattering cross section is simply proportional to the number of electrons Z in the target atom, the pair production cross section is roughly proportional to Z^2 [11] and the photo-electric cross section is roughly proportional to Z^5 [12]. Compton scattering of photons with energies in the few MeV range can produce electrons with energies that are within about 250 keV of the incident photon energy. In photo-electric absorption the energy of the ejected electron is more

nearly that of the incident photon since binding energies for K-shell electrons are typically around 100 keV for even the heaviest elements.

For the energies discussed here ionization rather than bremsstrahlung dominates electron energy loss. The length scale characterizing the slowing of a relativistic electron via ionization is given by the familiar Bethe-Bloch equation

$$\frac{dE}{dx} \approx 0.3\,\mathrm{MeV}\frac{\rho}{1\,\mathrm{g/cm^3}}\frac{Z}{A}\left(10 + \ln\frac{E_{\mathrm{MeV}}^{3/2}}{Z^{0.9}}\right) \tag{2}$$

Here E_{MeV} is the electron energy in units of MeV, ρ is the density of the target material, A and Z represent the atomic mass and number of target atom. Eq. 2 neglects a modest dependence on density. We have also supposed here that the mean excitation energy of the target atoms is $16Z^{0.9}$ eV, which is accurate to within about 10% for most elements heavier than hydrogen [13]. This equation implies that electrons will lose 1 MeV of their initial energy after traveling a distance L_{slow} given by

$$\rho L_{\mathrm{slow}} \approx 0.3\,\mathrm{g/cm^2}\frac{A}{Z}. \tag{3}$$

Here we have neglected the logarithmic dependence on electron energy and Z. From Eqs. 1 and 3 we see that photons can penetrate to a much greater depth than can electrons.

Bremsstrahlung emission by relativistic electrons favors the direction of the slowing electron and falls off with a characteristic angle of $1/\gamma$, where γ is the Lorentz factor of the electrons. As well, relativistic electrons born in Compton scattering and photo-absorption events tend to have an initial momentum along the direction of the incident photon. For this reason efficient production of energetic backscattered photons requires some way to turn the electron around. This is accomplished through multiple Coulomb scatterings off of nuclei and to a lesser extent electrons in the target material. A basic account of the process is presented in [14] and [15].

After traveling a distance x the mean deviation in angle $\langle(\Delta\theta)^2\rangle$ characterizing the direction of an electron is

$$\langle(\Delta\theta)^2\rangle \approx 0.3\frac{x\rho}{\mathrm{g/cm^2}}\frac{Z^2}{AE_{\mathrm{MeV}}^2}\ln(200E_{\mathrm{MeV}}/Z^{1/3}). \tag{4}$$

Together with Eq. 2 this implies that electrons turn around ($\langle(\Delta\theta)^2\rangle \sim 2$) after losing an energy $\Delta E \approx 20\mathrm{MeV}(E_{\mathrm{MeV}}^2/Z\ln(200E/Z^{1/3}))$. Batra and Sehgal [16]

have studied the interplay between electron energy loss and isotropization in more detail and find that this simple estimate is too low by about a factor of two. A better approximation to experimental studies is

$$(\Delta E)_{\rm turn} \approx 40{\rm MeV}\frac{E^2_{\rm MeV}}{Z\ln(200E_{\rm MeV}/Z^{1/3})}, \tag{5}$$

for electron energies in the range of one to several MeV and provided that $E-(\Delta E)_{\rm turn}$ is not less than about 1 MeV.

Eq. 5 is interesting because it indicates that for many important cases electrons lose some, but not quite all, of their initial energy before turning around. For example, for 2 MeV electrons in gold $(\Delta E)_{\rm turn} \approx 400$ keV, while for 3 MeV electrons in gold $(\Delta E)_{\rm turn} \approx 900$ keV. This implies that the detailed interplay between electron energy loss and directional evolution is important. If by contrast we had found that $(\Delta E)_{\rm turn}$ were always very small or very large, then this interplay would not be important. In section 3.3 we will see that photon production through multi-step processes exhibits a pronounced dependence on energy and target composition. This results in part because of the sensitivity to the interplay between electron slowing and turning.

3 Effective Cross Sections

3.1 Definition of Effective Cross Sections

It is convenient to have a compact and simple representation for the probability that an incident photon creates an outgoing photon that has a given energy and angle. For discrete microscopic scattering this representation is provided by the familiar differential cross section. We will define a similar quantity, an "effective cross section", to describe production of photons through multi-step processes.

For a beam of photons in an initial channel i incident on a body the effective cross section for production of photons in a final channel j will be defined as

$$\sigma^{\rm eff}_{i\to j} = \sigma^{\rm tot}\frac{f_{i\to j}}{f_{\rm tot}}. \tag{6}$$

Here $f_{i\to j}$ is the number of photons in the final state j relative to the number of photons in the incident beam, or alternatively the efficiency for producing photons in the state j. In Eq. 6 $f_{\rm tot}$ is the fraction of photons that undergo interactions of any kind in the body. The quantity $\sigma^{\rm tot}$ appearing on the right

hand side of Eq.6 is taken to be the total microscopic cross section characterizing interaction of incident photons with individual atoms in the target object. With this choice our definition gives the true microscopic differential cross section in the limit where the target is a single atom or a very thin sheet. For an object comprised of several different elements the total cross section in the above equation would be defined as the average of the total cross section characterizing each species.

The definition in Eq. 6 allows a simple determination of the flux of background photons in terms of available quantities. Total photon interaction cross sections for all elements with stable isotopes are available from the National Institute of Standards and Technology[17]. The fraction $f_{\rm tot}$ of photons that interact in a body of width L is given by

$$f_{\rm tot} = 1 - \exp(-L/L_\gamma), \tag{7}$$

where L_γ is the photon mean free path from Eq. 1.

3.2 Details of Monte Carlo Calculations

Monte Carlo simulations using the MCNP5 code [18] were used to calculate the effective cross sections defined in Eq. 6. The simulation geometry is shown in figure 1 and consists of a pencil beam incident normally on a plane slab of material. Tallies of outgoing photons were collected on a sphere surrounding the slab and binned in energy and angle.

The MCNP5 code is able to transport electrons, positrons, photons, and neutrons for a wide range of materials and energies. The slowing-down and deflection of charged particles is handled by the "condensed random walk" method. In this approach, a large number of microscopic Coulomb collisions are lumped into macroscopic steps for computational efficiency. The production of knock-on electrons, fluorescence x-rays, and bremsstrahlung photons from charged particles is sampled at each step. In addition, positrons undergo annihilation into two 0.511 MeV back-to-back photons at the end of their tracks.

The photo-atomic interactions treated by the code are (i) photoelectric absorption including the production of characteristic x-rays and Auger electrons, (ii) Compton scattering with bound electron corrections, (iii) Rayleigh scattering, and (iv) pair production. Among the processes that are not implemented are: (i) Nuclear Thomson and Delbrück scattering, and (ii) NRF absorption and emission.

Photonuclear physics has recently been implemented in MCNP5 for several

isotopes. However except for ^{2}H and ^{9}Be, the thresholds are above the energy range (few MeV) of most NRF experiments. We do not consider photonuclear processes in this study.

We employed several variance reductions techniques to reduce statistical noise. Bremsstrahlung emission was artificially enhanced in the high energy tail, with correspondingly smaller statistical weight per particle. Secondly, incident photon were forced to collide in the target, helpful for thin slab geometries. The typical run time for each problem was a few hours on single-node AMD Opteron CPU.

3.3 Results for photon production

Effective cross sections describing the production of energetic back-scattered photons were calculated using the definition in Eq. 6 and the simulation geometry shown in Fig. 1. We studied a range of different materials (from nitrogen to uranium), different incident photon energies (0.5 to 8 MeV), and different target thicknesses (0.1 to 100 g/cm^2). Tables 1 to 4 present tabulated results for effective cross sections averaged over back-scattered angles. A discussion of the angular dependence, as well as of other characteristics of multi-step photon production, is given below.

- Energy Dependence

  Fig. 2 illustrates production of photons from a thick lead target. One of the most striking features of these multi-step processes is the very steep rise in photon production with decreasing outgoing photon energy, or alternatively with increasing difference between the incident and final state photon energy. For all incident photon energies described by Fig. 2 photon production increases approximately exponentially as the outgoing photon energy decreases. And, the e-folding length characterizing this rise is small. For incident photons with an energy of 4 MeV the effective cross section increases by a factor of 10 as the outgoing photon energy varies from 3.5 to 3.0 MeV. For incident photons with an energy of 2 MeV the photon production increases by a factor of about twenty as the outgoing photon energy varies from 2 to 1.5 MeV.
- Dependence on Target Material

  Fig. 3 illustrates the dependence of photon production on target thickness for incident photons with an energy of 4 MeV. For back-scattered photons with energies between about 1.5 and 3.5 MeV the effective photon production cross section scales approximately as the fourth power of the atomic number Z characterizing the target. For this very thick target the fraction of photons that interact is essentially unity. From our definition (Eq. 6) of the effective cross section we then find that Z dependence implies an efficiency

for backscattered photon production scaling as $f_f \propto Z^4/\sigma^{\rm tot} \propto Z^3$. Here we have made the approximation that the total atomic interaction cross section scales as atomic number, which is true to within a factor of two for the cases shown in Fig. 3.

Fig. 4 shows the dependence of photon production on target Z for incident photons with an energy of 2 MeV. As for 4 MeV photons, production at intermediate energies ($\approx 1.2 - 1.8$ MeV in this case), scales approximately as Z^4. The Z dependence of photon production near the incident energy and for energies less than one MeV is more complicated.

It is interesting to note that the efficiency for producing back-scattered photons depends much more strongly on Z than does the efficiency for conversion of electron energy to photon energy. In both thin and thick targets, the efficiency for conversion of energy in an incident electron beam through bremsstrahlung scales as the first power of Z, provided that radiative losses do not dominate the energy loss [4]. On the other hand, for photon production does not scale as strongly with Z as do the cross sections for photoelectric absorption and pair production. Both of these processes produce energetic electrons and scale approximately as Z^5 [12].

- Angular Dependence

  Figs. 5 and 6 illustrate the angular dependence of back-scattered radiation for thin and thick targets. For a thin target emission peaks toward the plane of the target (at smaller angles). This arises because bremsstrahlung emission is itself peaked toward forward directions. And, in a thin target electrons do not have a chance to change direction before escaping. The angular distribution is most pronounced for energetic photons. The effective cross section for emission of 3 MeV photons anti-parallel to an incident 4 MeV photon beam is about 4 times smaller than for photons in the plane of the target. For less energetic photons the angular distribution is more modest.

  For a thick target emission of photons parallel to the plane of the target is suppressed. This is illustrated in Fig. 6 and arises because photons traveling at small angles have to traverse large distances before escaping the target. The competition between attenuation resulting from this extra distance and the decreased production of photons traveling at large angles results in an energy distribution that is roughly flat at large angles. Towards the plane of the target the emission falls steeply. It should be noted that the present results apply for targets that are much wider than thick. For targets with small widths emission in the plane of the target is enhanced relative to the result shown in Fig. 6.

- Dependence on Target Thickness

  Production of gamma-rays through multi-step processes occurring as a body is irradiated by energetic photons depends on the thickness of the body. This is because both gamma-rays and energetic electrons travel macroscopic distances in even dense objects. In particular, for a very thin object electrons that are made energetic through collisions with incident pho-

tons do not have time to emit bremsstrahlung radiation before escaping the target. The efficiency for bremsstrahlung production increases with target thickness until the target is so thick that electrons are efficiently slowed. From Eq. 3 this is found to occur at an areal density $\rho L \approx 0.3 \mathrm{g/cm^2}(A/Z) \approx 0.6 \mathrm{g/cm^2}$. Note that this is much smaller than the distance traveled by MeV photons.

Fig. 7 illustrates the dependence of back-scattered photon production on target thickness for 4 MeV photons incident on lead. For a very thin target (0.1 g/cm^2), for which energetic electrons do not have time to radiate before escaping, photon production is suppressed. Once the target thickness reaches 1 g/cm^2 the effective cross section is close to reaching a plateau. This implies that for all but the thinnest lead samples one can take the infinitely thick result as a fair approximation to the effective cross section. Note that the effective cross section for a very thick target is actually a little smaller than for intermediate areal densities. This arises because of self attenuation. Photons produced deep within the lead have a smaller chance of making it out.

It is evident from Fig. 7 that the dependence of photon production on target thickness becomes less pronounced with increasing outgoing photon energy. This occurs because the most energetic photons must come from electrons that have not traveled large distances. From Eq. 2 we see that an electron traveling in lead loses about 200 keV for every 0.1 g/cm^2 of areal density traversed.

4 Comparison with Elastic Processes

Like multi-step processes, elastic scattering also contributes to the flux of high energy photons emitted at large angles relative to a beam incident on a target. Very little of a photon's energy is lost during an elastic collision with an atom. For this reason elastic processes will always dominate production of backscattered radiation at energies very near the incident energy. But for a range of outgoing energies larger than some minimum, multi-step processes will dominate the photon production.

To motivate an understanding of the competition between multi-step scattering and elastic scatterings we first consider elastic Rayleigh scattering. This is the dominant elastic process for photons with energies smaller than about 1 MeV. As noted above, our Monte Carlo calculations and definitions of effective cross sections include Rayleigh scattering. In our calculations this elastic process is responsible for the effective cross section at outgoing energies very near the incident energy. For example, from Table 3 we see that the effective cross section in the last outgoing energy bin (1.95 MeV) for 2 MeV photons incident on lead is 0.05μb/(sr keV). Since these values are averaged over bins that are 100 keV wide, and since Rayleigh scattering itself results in a very small change in the scattered photon energy, we

have to multiply this result by 100 keV to recover the Rayleigh scattering cross section. The result is approximately 5 μb/sr for large angle Rayleigh scattering.

It is clear from the tables and figures that multi-step processes overwhelmingly dominate over Rayleigh scattering for production of photons within a few hundred keV of the incident energy. Again using the example of 2 MeV photons incident on a thin lead target, we see from Table 3 that the number of backscattered photons produced with energies within 300 keV of the incident energy is about five times larger than the number produced by Rayleigh scattering alone. For a thick lead target the ratio is about twice as large. Of course, Rayleigh scattering can still be readily observed with monoenergetic sources and high resolution detectors because it is characterized by a nearly mono-energetic photon, whereas photons from the multi-step backgrounds are spread out in energy.

For photon energies larger than about one MeV the large angle Rayleigh scattering cross section is a poor approximation to the total large angle elastic scattering. Other processes like Delbrück and Nuclear Thomson scattering add coherently with Rayleigh scattering. At high incident photon energies these dominate the large angle elastic scattering. As a first approximation one can approximate the total elastic cross section at energies between about 2 and 5 MeV by classical nuclear Thomson scattering

$$\frac{d\sigma^{\rm NT}}{d\Omega} \approx 30 \frac{\mu{\rm b}}{\rm sr} \left(\frac{Z}{92}\right)^4 \left(\frac{238}{A}\right)^2 \left(\frac{1+\cos^2\theta}{2}\right), \tag{8}$$

which is independent of initial photon energy. From Tables 3 and 4 we see that for 2 MeV photons incident on lead or uranium, multi-step processes dominate over nuclear Thomson scattering for energy ranges wider than about 200 keV. For 4 MeV incident photons nuclear Thomson scattering dominates net production of backscattered photons for outgoing photons with energies within about 500 keV of the incident energy.

5 Implications for NRF experiments

5.1 Basic Estimates

In NRF experiments a γ-ray beam is shined on a target foil. This foil is typically chosen to have an optical depth to resonant photons near unity, or an areal density of one to a few g/cm^2. In this case the relevant cross sections for multi-step processes are those for thick targets.

Typical NRF cross sections for strong resonances in heavy elements are usu-

ally of the same size as cross sections characterizing atomic interactions. In well studied uranium isotopes, for example, the cross sections for resonant absorption and re-emission of photons are near $d\sigma^{\rm NRF}/d\Omega = 1$b/sr [19]. This is very large compared to cross sections for elastic scattering and multi-step processes. However, NRF is also characterizing by small effective widths. For actinides and other heavy elements the thermally averaged widths are [2]

$$\Gamma_{\rm NRF} \approx 1\,{\rm eV}\left(\frac{E_{\rm res}}{1\,{\rm MeV}}\right), \tag{9}$$

where $E_{\rm res}$ is the energy of the resonant nuclear state. Only incident photons within approximately $\Gamma_{\rm NRF}$ of the resonant energy can excite nuclear transitions.

Widths characterizing the energy resolution of beams used in NRF experiments are always much larger than $\Gamma_{\rm NRF}$. Bremsstrahlung sources have approximately flat power spectra and are characterized by an energy width $\Gamma_{\rm beam} \sim 1$ MeV. Next generation laser/linac sources based on Thomson upscattering of laser light are calculated to have energy widths near 1 keV [9,10], which is still a thousand times larger than the NRF widths. Though cross sections for production of high energy backscattered photons are small, an appreciable fraction of the incident beam can contribute to these photons.

To see under what conditions an NRF experiment becomes dominated by multi-step backgrounds we first consider experiments with beams characterized by fine energy resolution. For these sources the energy resolution of the detector (Γ_d) will be poorer than that of the beam. The ratio of NRF counts to background counts is given by

$$\frac{N_{\rm NRF}}{N_{\rm B}} = \frac{\Gamma_{\rm NRF}(d\sigma^{\rm NRF}/d\Omega)}{\Gamma_d\langle d\sigma^{\rm eff}/d\Omega\rangle}. \tag{10}$$

Here $\langle d\sigma^{\rm eff}/d\Omega\rangle$ is the cross section for multi-step processes averaged over the energy resolution of the detector. From Table 4 we see that even for heavy elements, where multi-step processes are most important, the detector resolution can be very poor before multi-step backgrounds become important. For 2 MeV photons on uranium the ratio of background counts to NRF counts does not approach unity until $\Gamma_d \approx 1$ MeV. For detector resolutions typical of HPGe or NaI only elastic processes need be considered for backgrounds.

Experiments using bremsstrahlung sources typically use HPGe detectors characterized by an energy resolution of a few keV. For these experiments one is typically concerned with the shape of the background as a function of distance in energy away from the beam endpoint energy. This determines the smallest resonance energies that can be observed for a given endpoint.

The intensity of background radiation at energy E' resulting from a broad-band beam incident on a foil is

$$\frac{d\phi}{dE'd\Omega} \propto \int_{E'}^{E_{\rm end}} \frac{d\sigma^{\rm eff}}{d\Omega dE'} \frac{d\phi_{\rm beam}}{dE} dE. \tag{11}$$

Here ϕ represents photon flux, $\phi_{\rm beam}$ corresponds to the flux in the incident beam, E represents incident photon energy, and $E_{\rm end}$ represents the beam endpoint or maximum energy of photons in the beam. The figures and Table 4 show that over a modest energy range the effective cross section rises approximately exponentially with increasing distance between the incident and outgoing photon energies. This suggests

$$\frac{d\sigma^{\rm eff}}{d\Omega dE'}(E, E') \approx \frac{d\sigma^{\rm eff}}{d\Omega dE'}(E = E_{\rm end}, E') \times e^{-(E_{\rm end}-E)/s_E}, \tag{12}$$

where s_E is the energy scale characterizing the rise of the effective cross section with increasing distance between the incident and outgoing photon energies. Figures 3 and 4 show that for incident photons with energies between 2 and 4 MeV and for elements spanning the range from nitrogen to uranium

$$s_E \approx 200 - 400\,{\rm keV} \tag{13}$$

over a broad range of energies. Since bremsstrahlung photon beams usually don't vary much over this small an energy scale we can approximate the integral in Eq.11 as

$$\frac{d\phi}{dE'd\Omega} \propto s_E \frac{d\sigma^{\rm eff}}{d\Omega dE'}(E = E_{\rm end}, E') \frac{d\phi_{\rm beam}}{dE}(E = E'). \tag{14}$$

With this the ratio of counts in the NRF peak to background counts from multi-step processes is

$$\frac{N_{\rm NRF}}{N_{\rm B}} \approx 10 \left(\frac{\Gamma_d}{1\,{\rm keV}}\right) \left(\frac{\Gamma_{\rm NRF}}{1\,{\rm eV}}\right) \left(\frac{100\,{\rm keV}}{s_E}\right) \left(\frac{d\sigma^{\rm NRF}/d\Omega}{1{\rm b/sr}}\right) \left(\frac{1\mu{\rm b/sr\,keV}}{d\sigma^{\rm eff}/d\Omega dE'}\right). \tag{15}$$

Here the effective cross section is understood to be evaluated at $E = E_{\rm end}$, $E' = E_{\rm res}$. In experiments with high Z targets the ratio in Eq. 15 approaches unity once this effective cross section reaches $\sim 1 - 10\mu{\rm b/(sr\ keV)}$. The exact value depends on the strength of the NRF transition and on the detector resolution. For a 2 MeV endpoint machine it is seen from Table 4 that multi-step processes can become problematic for resonance energies below about 1500 keV. For a 4 MeV endpoint machine the energy window in which resonances can be easily detected is about twice as large.

To illustrate the calculations of backgrounds presented above we show in Fig. 8 spectra of back-scattered photons resulting from broad-band beams incident on a thick uranium target. For simplicity we have supposed the incident beam to be characterized by a flat power spectrum, or a flux inversely proportional to energy. Different spectra in Fig. 8 correspond to different choices for the beam endpoint energy $E_{\rm end}$. In each case the back-scattered flux has been divided by the flux in the incident beam at an energy of 2 MeV.

For the same geometry described above we also studied the strength of a back-scattered signal resulting from NRF interactions. The resonance energy was taken to be 2 MeV, the NRF cross section to be 1 b/sr, and the thermally averaged width of the resonance was assumed as 1 eV. Emission of 2 MeV photons following de-excitation of an excited nucleus was approximated as being isotropic and characterized by a branching ratio of unity. Through simulations the efficiency for a resonant photon incident on the foil to result in a 2 MeV photon exiting the foil in the backwards direction was found to be 0.092.

The vertical line at 2 MeV in Fig. 8 shows the flux of back-scattered NRF photons. This assumes that the NRF line is spread out over an energy of 4 keV, which is approximately characteristic of the resolution of high purity germanium detectors at this energy. It is seen that for this energy resolution and a beam endpoint energy of 2.5 MeV (which is 500 keV above the resonance energy), the ratio of counts in the background to counts in the NRF line is about one. For a beam endpoint energy an MeV higher than the resonance energy, the ratio of counts in the background to counts in the NRF line is about six. With a beam endpoint energy of 4 MeV the ratio is approximately thirty.

6 Summary

We have presented calculations describing photon production through multi-step processes occurring when a beam of gamma-rays is shined on a macroscopic material. These processes give rise to energetic photons traveling at large angles relative to the incident gamma-ray beam. Over a fairly broad energy range the spectrum of back-scattered photons rises approximately exponentially with increasing energy. For energies greater than the electron rest mass and smaller than a few hundred keV less than the incident energy, multi-step processes dominate the production of back-scattered photons.

Experiments observing Nuclear Resonance Fluorescence with broadband bremsstrahlung

beams are particularly sensitive to these multi-step processes. Because of the nearly exponential rise of background with decreasing energy, resonance lines can only be observed near the beam endpoint energy. Our calculations can be used to quantify backgrounds and signals expected in NRF and other experiments involving the observation of $\gamma-$rays scattered at large angles relative to a beam incident on a material.

7 Acknowledgements

This work was performed under the auspices of the U.S. Department of Energy by the University of California, Lawrence Livermore National Laboratory under Contract No. W-7405-ENG-48.

References

[1] Schiff, L. I., Phys. Rev., 70, 761 (1946).

[2] Metzger, F.R., Phys. Rev., 101, 286 (1956).

[3] Kneissl, U., Pitz, H.H. & Zilges, A., Prog. Part. Nucl. Phys., 37, 349 (1996).

[4] Koch, H. W. & Motz, J. W., Rev. Mod. Phys., 31, 920 (1959).

[5] Rullhusen, P., Zurmühl, U., Mückenheim, W., Smend, F. & Schumacher, M., Nucl. Phys. A, 382, 79 (1982).

[6] Pruet, J., McNabb, D.M., Hagmann, C., Hartemann, F.V. & Barty, C.P.J., J. Appl. Phys., 99, 123102 (2006).

[7] Chatterjee, B. K. & Roy, S. C., J. Phys. Chem. Ref. Data, 98, 1011 (1998).

[8] Kissel, L., Rad. Phys. and Chem. 59, 185 (2000). An electronic version of elastic scattering cross sections is available at http://www-pat.llnl.gov/Research/scattering/RTAB.html.

[9] Barty, C.P.J. & Hartemann, Lawrence Livermore Laboratory Report, UCRL-TR-206825 (2004).

[10] Hartemann, F.V., Brown, W.J., Gibson, D.J., Anderson, S.G., Tremaine, A.M., Springer, P.T., Wootton, A.J., Hartouni, E.P. & Barty, C.P.J., Phys. Rev. ST Accel. Beams, 8, 100702 (2005).

[11] Bethe, H. A. & Heitler, W., Proc. Royal Soc., 146A, 83 (1934).

[12] Bethe, H. A. & Maximon, L. C., Phys. Rev., 93, 768 (1954).

[13] Eidelman, S. et al., Phys. Lett. B, 592, 1 (2004).

[14] Scott, W., Rev. Mod. Phys., 35, 231 (1963).

[15] Jackson, J. D., "Classical Electrodynamics", Wiley & Sons (1975).

[16] Batra, R. K. & Sehgal, M. L., Phys. Rev. B, 23, 4448 (1981).

[17] National Institute of Standards and Technology web-site, (2006), http://physics.nist.gov/PhysRefData/Xcom/Text/XCOM.html.

[18] MCNP "A General Monte Carlo N-Particle Transport Code", Version 5, X-5 Monte Carlo Team, LA-UR-03-1987 (2003).

[19] Margraf, J. Degener, A., Friedrichs, H., Heil, R. D., Jung, A., Kneissl, U., Lindenstruth, S., Pitz, H. H., Schacht, H., Seemann, U., Stock, R. & Wesselborg, C., Phys. Rev. C, 42, 771 (1990).

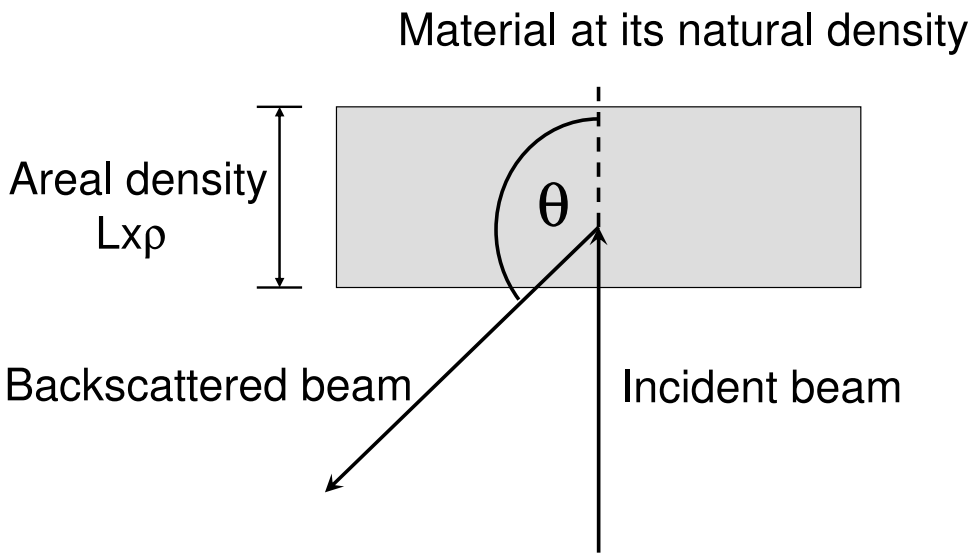

Fig. 1. Geometry used in the Monte Carlo simulations. For nitrogen we used a density of $1 g/cm^3$. For all other elements we used typical natural densities.

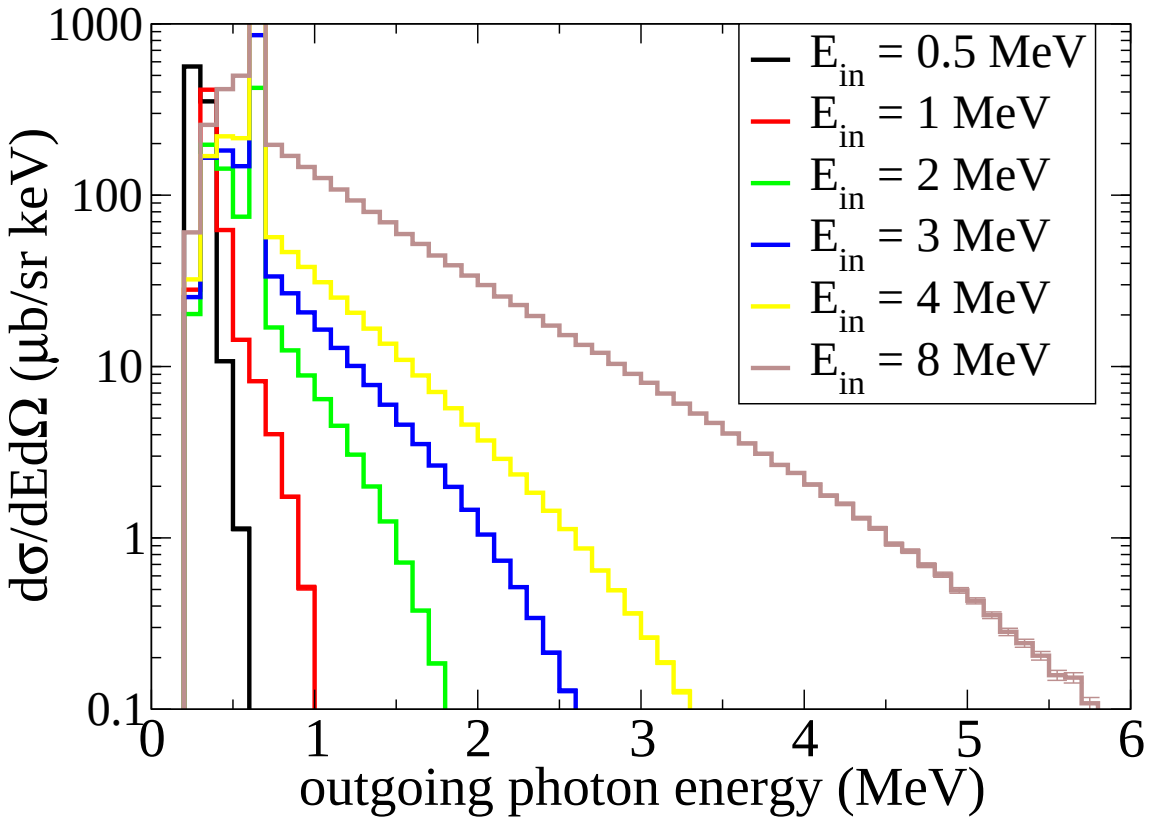

Fig. 2. Illustration of the energy dependence of processes that produce high energy backscattered photons. The target here is a thick (100 g/cm^2) lead foil and different lines correspond to different incident photon energies. The effective cross section here has been averaged over all backwards angles.

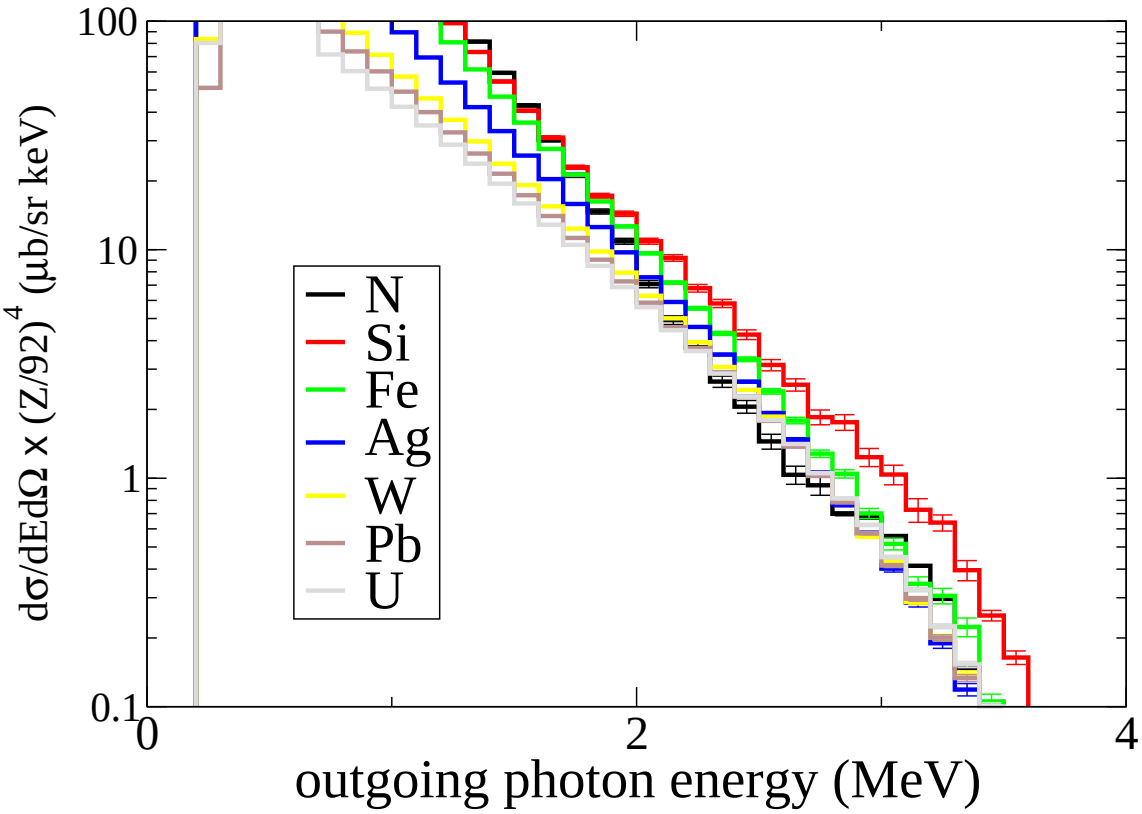

Fig. 3. Effective cross section for production of high energy backscattered photons for different target materials. To illustrate the dependence of photon production on Z we have multiplied each cross section by the ratio of the target Z to the atomic number for uranium to the fourth power. All targets here have an areal density of 100 g/cm^2. The incident photon energy here is 4 MeV and the effective cross section has been averaged over all backwards angles.

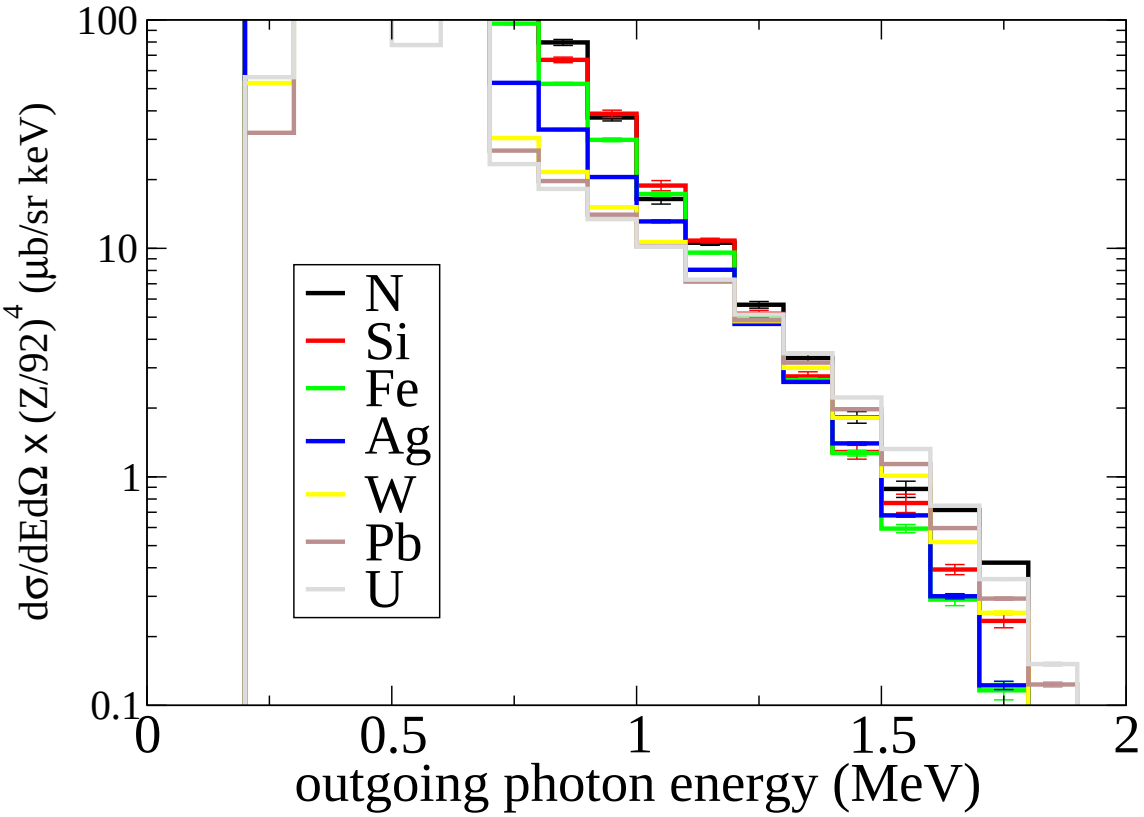

Fig. 4. Same as figure 3 except here the photons have an incident energy of 2 MeV rather than 4 MeV.

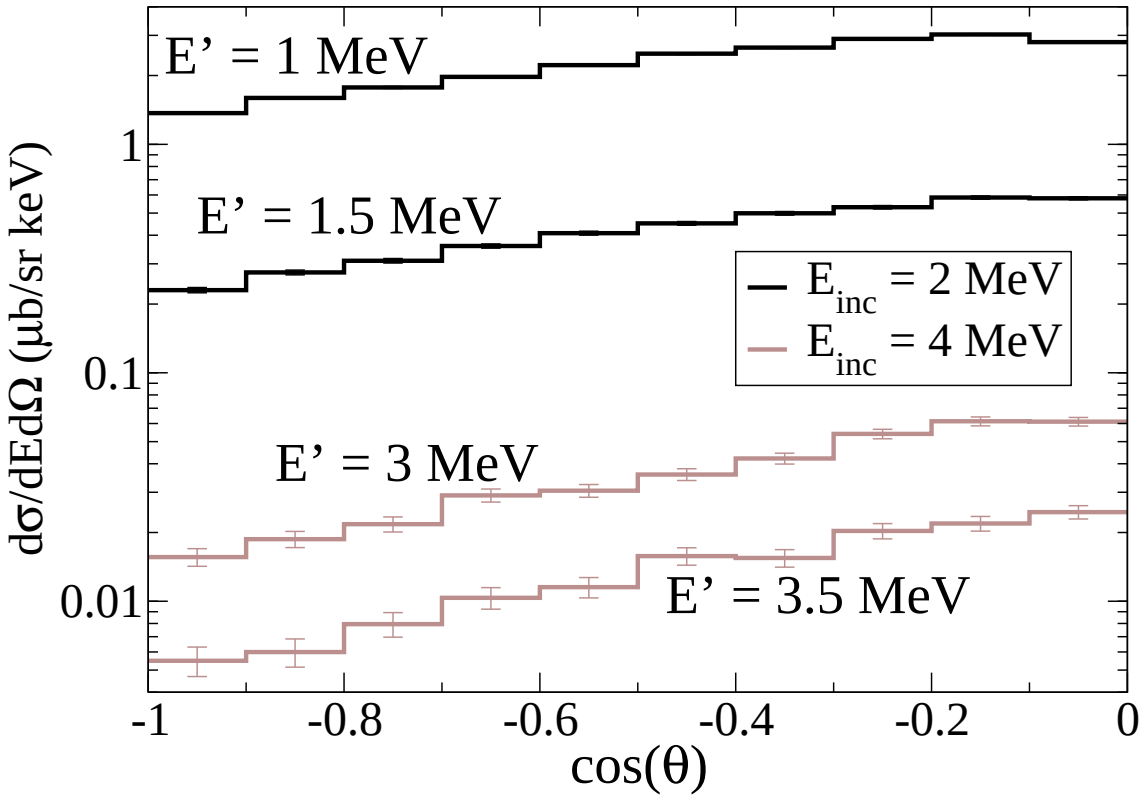

Fig. 5. Dependence of photon production on angle of emission for a thin lead target (0.1 g/cm^2). Here $\cos(\theta) = -1$ corresponds to background photons emitted anti-parralel to a beam incident normally on the target while $\cos(\theta) = 0$ corresponds to photons that are emitted perpendicularly to the incident beam. The width of the angular bins here is given by $\Delta\cos(\theta) = 0.1$.

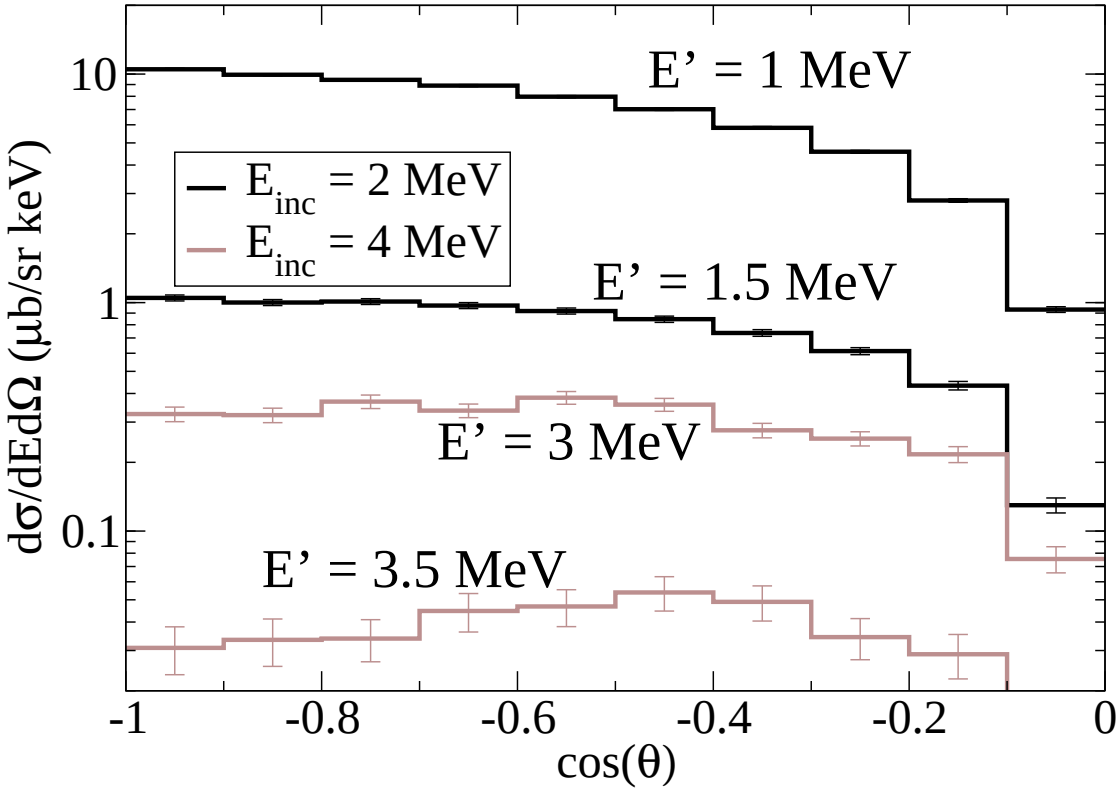

Fig. 6. Dependence of photon production on angle of emission for a thick lead target (100 g/cm^2). Here $\cos(\theta) = -1$ corresponds to background photons emitted anti-parralel to a beam incident normally on the target while $\cos(\theta) = 0$ corresponds to photons that are emitted perpendicularly to the incident beam. The width of the angular bins here is given by $\Delta\cos(\theta) = 0.1$.

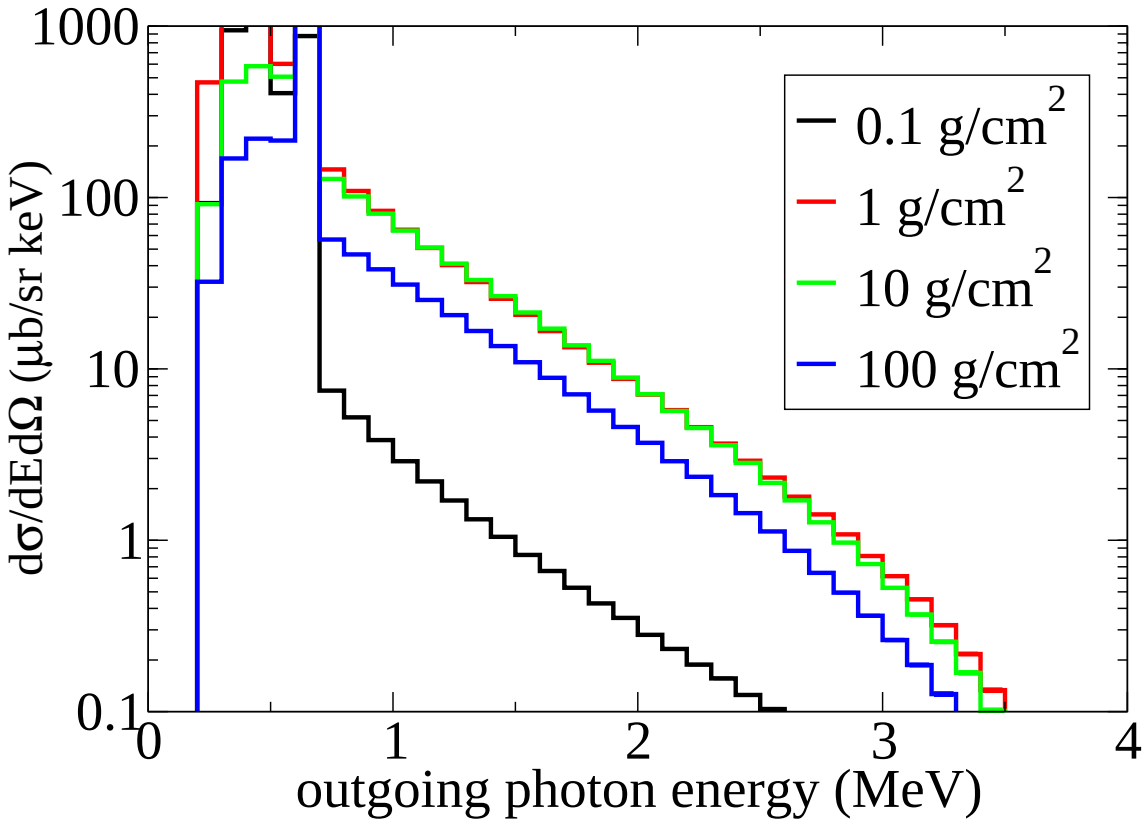

Fig. 7. Illustration of the dependence of backscattered photon production on thickness of the target object. The target here is comprised of lead and different lines correspond to different areal densities for this target. The energy of the incident photon here is 4 MeV and the effective cross section has been averaged over all backwards angles.

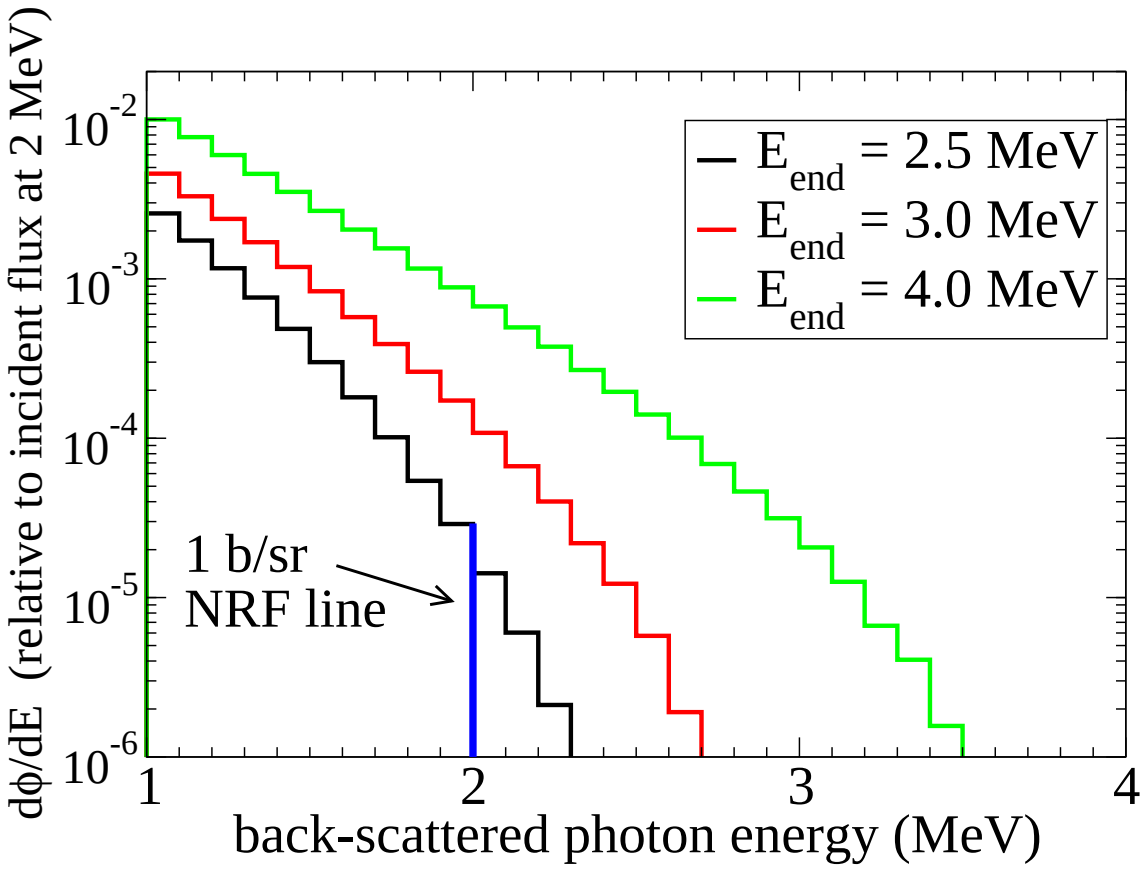

Fig. 8. Spectra of back-scattered photons resulting from broad-band beams incident on a thick uranium target. Here the target has an areal density of 1000 g/cm^2 and the incident beam is assumed to have a flat power spectrum. Different curves correspond to different beam enpoint energies ($E_{\rm end}$). For each case the flux in the incident beam at 2 MeV is assumed to be unity. The blue line at 2 MeV corresponds to the flux from an NRF resonance characterized by a cross section of 1 b/sr. This line is assumed to be spread out over an energy of 4 keV, which is approximately characteristic of the resolution of high purity germanium detectors at this energy.

Table 1
Effective Photon Production Cross Sections (μb/sr·keV) for Low Energy Photons Incident on Thin Targets (0.1 g/cm^2).

$E_{\rm in}$(MeV)	$E_{\rm out}$(MeV)	N	Fe	Pb
0.50	0.15	4.85e+02	1.80e+03	5.59e+03
0.50	0.25	5.10e+02	1.89e+03	5.15e+03
0.50	0.35	4.84e-02	2.14e-01	3.95e+01
0.50	0.45	1.32e-06	8.14e-03	3.37e+00
1.00	0.15	7.32e+00	3.30e+01	2.41e+02
1.00	0.25	5.01e+02	1.86e+03	5.65e+03
1.00	0.35	1.24e+02	4.60e+02	1.27e+03
1.00	0.45	1.23e-01	7.26e-01	2.53e+01
1.00	0.55	8.95e-04	1.04e-01	1.31e+01
1.00	0.65	3.06e-04	3.03e-02	6.76e+00
1.00	0.75	1.05e-04	5.85e-03	3.24e+00
1.00	0.85	1.24e-07	7.21e-04	1.19e+00
1.00	0.95	4.18e-08	2.88e-04	1.32e-01

Table 2
Effective Photon Production Cross Sections (μb/sr·keV) for Low Energy Photons Incident on Thick Targets (100 g/cm^2).

$E_{\rm in}$(MeV)	$E_{\rm out}$(MeV)	N	Fe	Pb
0.50	0.15	6.18e+02	1.31e+03	5.63e+02
0.50	0.25	1.55e+02	4.83e+02	3.53e+02
0.50	0.35	1.39e-01	4.90e-01	1.07e+01
0.50	0.45	4.35e-07	2.80e-03	1.13e+00
1.00	0.15	2.18e+02	3.62e+02	2.81e+01
1.00	0.25	2.32e+02	7.40e+02	4.12e+02
1.00	0.35	2.11e+01	7.26e+01	6.26e+01
1.00	0.45	4.29e-01	1.73e+00	1.43e+01
1.00	0.55	2.10e-03	7.27e-02	8.21e+00
1.00	0.65	1.49e-04	1.63e-02	4.03e+00
1.00	0.75	2.67e-05	2.82e-03	1.74e+00
1.00	0.85	2.47e-08	3.32e-04	5.12e-01
1.00	0.95	1.89e-08	1.01e-04	5.53e-02

Table 3: Effective Photon Production Cross Sections (μb/sr·keV) for multi-MeV Photons Incident on Thin Targets (0.1 g/cm^2)

E_{in}(MeV)	E_{out}(MeV)	N	Si	Fe	Ag	W	Pb	U
2.00	0.15	3.00e+00	6.62e+00	1.47e+01	4.02e+01	1.04e+02	1.33e+02	5.28e+02
2.00	0.25	1.93e+02	3.87e+02	7.19e+02	1.30e+03	2.02e+03	2.24e+03	2.50e+03
2.00	0.35	1.74e+02	3.50e+02	6.50e+02	1.17e+03	1.78e+03	1.96e+03	2.15e+03
2.00	0.45	6.79e+00	1.38e+01	2.63e+01	4.80e+01	7.15e+01	7.85e+01	8.82e+01
2.00	0.55	3.94e+00	1.78e+01	6.87e+01	2.75e+02	8.88e+02	1.19e+03	1.62e+03
2.00	0.65	9.83e-04	1.22e-02	1.08e-01	8.94e-01	4.52e+00	6.76e+00	1.06e+01
2.00	0.75	4.69e-04	6.73e-03	6.50e-02	5.64e-01	3.02e+00	4.53e+00	7.26e+00
2.00	0.85	2.96e-04	3.87e-03	3.87e-02	3.71e-01	2.08e+00	3.12e+00	5.14e+00
2.00	0.95	1.58e-04	2.49e-03	2.56e-02	2.48e-01	1.48e+00	2.27e+00	3.76e+00
2.00	1.05	1.07e-04	1.47e-03	1.58e-02	1.69e-01	1.07e+00	1.65e+00	2.82e+00
2.00	1.15	7.40e-05	1.04e-03	1.01e-02	1.14e-01	7.62e-01	1.22e+00	2.10e+00
2.00	1.25	4.87e-05	5.72e-04	6.43e-03	7.39e-02	5.43e-01	8.76e-01	1.56e+00
2.00	1.35	4.15e-05	4.35e-04	3.82e-03	4.71e-02	3.76e-01	6.24e-01	1.15e+00
2.00	1.45	3.47e-05	2.93e-04	2.59e-03	2.88e-02	2.50e-01	4.25e-01	8.18e-01
2.00	1.55	3.42e-05	2.34e-04	1.66e-03	1.69e-02	1.55e-01	2.76e-01	5.47e-01
2.00	1.65	3.23e-05	2.49e-04	1.38e-03	1.03e-02	9.49e-02	1.70e-01	3.43e-01
2.00	1.75	9.95e-06	6.40e-05	3.67e-04	3.82e-03	4.60e-02	8.78e-02	1.82e-01
2.00	1.85	-	-	4.20e-05	1.33e-03	2.60e-02	5.00e-02	8.80e-02
2.00	1.95	-	-	-	9.26e-04	8.45e-03	8.86e-03	1.67e-02
3.00	0.15	1.89e+00	4.18e+00	9.54e+00	2.89e+01	8.46e+01	1.11e+02	3.50e+02
3.00	0.25	1.14e+02	2.27e+02	4.22e+02	7.66e+02	1.21e+03	1.35e+03	1.51e+03
3.00	0.35	1.24e+02	2.48e+02	4.61e+02	8.33e+02	1.30e+03	1.43e+03	1.59e+03
3.00	0.45	3.22e+01	6.42e+01	1.20e+02	2.16e+02	3.25e+02	3.53e+02	3.83e+02
3.00	0.55	4.33e+00	1.96e+01	7.48e+01	2.86e+02	8.33e+02	1.07e+03	1.40e+03
3.00	0.65	1.38e-02	3.74e-02	1.44e-01	9.42e-01	5.01e+00	7.53e+00	1.18e+01
3.00	0.75	1.03e-03	8.64e-03	6.70e-02	5.87e-01	3.41e+00	5.18e+00	8.18e+00
3.00	0.85	7.29e-04	5.69e-03	4.63e-02	4.08e-01	2.43e+00	3.69e+00	5.92e+00
3.00	0.95	5.49e-04	4.02e-03	3.25e-02	2.89e-01	1.74e+00	2.68e+00	4.29e+00
3.00	1.05	4.02e-04	3.22e-03	2.20e-02	2.05e-01	1.28e+00	1.97e+00	3.18e+00
3.00	1.15	3.30e-04	2.19e-03	1.61e-02	1.50e-01	9.37e-01	1.45e+00	2.39e+00
3.00	1.25	2.79e-04	1.82e-03	1.19e-02	1.11e-01	7.05e-01	1.10e+00	1.80e+00
3.00	1.35	2.16e-04	1.40e-03	8.47e-03	8.02e-02	5.23e-01	8.22e-01	1.35e+00
3.00	1.45	1.30e-04	1.02e-03	6.98e-03	6.12e-02	3.95e-01	6.25e-01	1.03e+00
3.00	1.55	8.42e-05	9.07e-04	5.42e-03	4.60e-02	3.07e-01	4.78e-01	7.96e-01
3.00	1.65	3.43e-05	6.69e-04	4.12e-03	3.52e-02	2.34e-01	3.69e-01	6.08e-01
3.00	1.75	1.88e-05	5.85e-04	2.92e-03	2.70e-02	1.82e-01	2.80e-01	4.81e-01
3.00	1.85	1.68e-05	4.96e-04	2.71e-03	2.11e-02	1.42e-01	2.25e-01	3.83e-01
3.00	1.95	1.37e-05	4.30e-04	2.33e-03	1.70e-02	1.16e-01	1.83e-01	3.13e-01
3.00	2.05	1.15e-05	3.69e-04	1.94e-03	1.40e-02	9.04e-02	1.48e-01	2.65e-01
3.00	2.15	1.04e-05	4.44e-04	1.70e-03	1.18e-02	7.57e-02	1.21e-01	2.14e-01
3.00	2.25	1.03e-05	3.42e-04	1.60e-03	9.87e-03	6.16e-02	9.46e-02	1.75e-01
3.00	2.35	9.34e-06	2.91e-04	1.55e-03	8.73e-03	4.79e-02	7.68e-02	1.37e-01
3.00	2.45	9.89e-06	2.74e-04	1.32e-03	7.36e-03	3.87e-02	6.30e-02	1.11e-01
3.00	2.55	1.07e-05	2.67e-04	1.25e-03	5.49e-03	2.95e-02	4.66e-02	8.25e-02
3.00	2.65	1.14e-05	2.00e-04	9.51e-04	4.20e-03	2.07e-02	3.18e-02	5.83e-02
3.00	2.75	3.19e-06	2.90e-05	1.91e-04	1.14e-03	8.42e-03	1.57e-02	3.08e-02

Continued on next page

Table 3 – continued from previous page

E_{in}(MeV)	E_{out}(MeV)	N	Si	Fe	Ag	W	Pb	U
3.00	2.85	-	-	-	-	6.39e-03	1.33e-02	2.37e-02
3.00	2.95	-	-	-	-	3.12e-03	2.89e-03	5.14e-03
4.00	0.15	1.38e+00	3.05e+00	7.07e+00	2.26e+01	7.04e+01	9.28e+01	2.65e+02
4.00	0.25	7.94e+01	1.59e+02	2.95e+02	5.35e+02	8.52e+02	9.46e+02	1.07e+03
4.00	0.35	9.59e+01	1.91e+02	3.56e+02	6.43e+02	1.01e+03	1.11e+03	1.24e+03
4.00	0.45	3.66e+01	7.30e+01	1.37e+02	2.45e+02	3.74e+02	4.06e+02	4.45e+02
4.00	0.55	3.94e+00	1.78e+01	6.73e+01	2.50e+02	6.95e+02	8.75e+02	1.12e+03
4.00	0.65	2.31e-02	5.53e-02	1.66e-01	9.33e-01	4.98e+00	7.47e+00	1.18e+01
4.00	0.75	1.27e-03	8.67e-03	6.20e-02	5.64e-01	3.46e+00	5.21e+00	8.37e+00
4.00	0.85	8.15e-04	5.91e-03	4.29e-02	4.07e-01	2.51e+00	3.84e+00	6.14e+00
4.00	0.95	6.10e-04	4.49e-03	3.22e-02	2.96e-01	1.89e+00	2.89e+00	4.67e+00
4.00	1.05	5.07e-04	3.35e-03	2.39e-02	2.22e-01	1.44e+00	2.20e+00	3.61e+00
4.00	1.15	4.34e-04	2.63e-03	1.78e-02	1.69e-01	1.10e+00	1.71e+00	2.79e+00
4.00	1.25	3.41e-04	2.14e-03	1.50e-02	1.27e-01	8.48e-01	1.33e+00	2.19e+00
4.00	1.35	2.85e-04	1.80e-03	1.11e-02	9.95e-02	6.71e-01	1.05e+00	1.72e+00
4.00	1.45	2.28e-04	1.40e-03	9.21e-03	7.85e-02	5.22e-01	8.21e-01	1.37e+00
4.00	1.55	1.75e-04	1.22e-03	7.32e-03	6.18e-02	4.18e-01	6.61e-01	1.09e+00
4.00	1.65	1.45e-04	9.59e-04	6.10e-03	5.30e-02	3.40e-01	5.28e-01	8.91e-01
4.00	1.75	1.07e-04	8.06e-04	5.10e-03	4.12e-02	2.76e-01	4.28e-01	7.18e-01
4.00	1.85	1.00e-04	6.45e-04	4.01e-03	3.23e-02	2.24e-01	3.52e-01	5.80e-01
4.00	1.95	6.63e-05	6.53e-04	3.69e-03	2.66e-02	1.76e-01	2.81e-01	4.78e-01
4.00	2.05	4.97e-05	5.59e-04	3.00e-03	2.28e-02	1.46e-01	2.32e-01	3.82e-01
4.00	2.15	3.11e-05	4.51e-04	2.65e-03	1.90e-02	1.18e-01	1.88e-01	3.21e-01
4.00	2.25	1.28e-05	4.31e-04	2.40e-03	1.51e-02	9.92e-02	1.56e-01	2.59e-01
4.00	2.35	1.04e-05	4.01e-04	1.92e-03	1.27e-02	8.05e-02	1.25e-01	2.13e-01
4.00	2.45	8.75e-06	3.09e-04	1.81e-03	1.14e-02	6.66e-02	1.04e-01	1.68e-01
4.00	2.55	6.64e-06	3.03e-04	1.31e-03	9.01e-03	5.23e-02	8.40e-02	1.44e-01
4.00	2.65	5.59e-06	2.51e-04	1.09e-03	7.03e-03	4.23e-02	6.81e-02	1.18e-01
4.00	2.75	4.92e-06	2.29e-04	9.94e-04	5.65e-03	3.60e-02	5.72e-02	9.79e-02
4.00	2.85	5.28e-06	2.03e-04	8.34e-04	4.73e-03	2.86e-02	4.55e-02	7.48e-02
4.00	2.95	4.16e-06	1.64e-04	6.73e-04	4.07e-03	2.32e-02	3.75e-02	6.35e-02
4.00	3.05	3.58e-06	1.41e-04	6.59e-04	3.35e-03	1.88e-02	3.31e-02	5.18e-02
4.00	3.15	3.29e-06	1.57e-04	6.80e-04	2.78e-03	1.71e-02	2.70e-02	4.61e-02
4.00	3.25	2.24e-06	1.19e-04	4.96e-04	2.64e-03	1.40e-02	2.20e-02	3.78e-02
4.00	3.35	1.63e-06	1.03e-04	4.34e-04	2.28e-03	1.23e-02	1.99e-02	3.18e-02
4.00	3.45	1.26e-06	8.19e-05	3.59e-04	1.51e-03	7.82e-03	1.23e-02	2.38e-02
4.00	3.55	1.14e-06	7.04e-05	3.21e-04	1.42e-03	6.39e-03	1.02e-02	1.74e-02
4.00	3.65	1.07e-06	3.65e-05	1.69e-04	6.50e-04	3.11e-03	6.56e-03	1.27e-02
4.00	3.75	2.10e-07	3.27e-06	1.40e-05	1.57e-04	1.57e-03	3.04e-03	6.50e-03
4.00	3.85	-	-	-	6.82e-05	1.27e-03	1.96e-03	2.94e-03
4.00	3.95	-	-	-	5.40e-05	3.34e-04	2.69e-04	7.03e-04
8.00	0.15	6.53e-01	1.46e+00	3.49e+00	1.23e+01	4.07e+01	5.45e+01	1.38e+02
8.00	0.25	3.48e+01	6.98e+01	1.30e+02	2.36e+02	3.78e+02	4.25e+02	4.83e+02
8.00	0.35	4.98e+01	9.97e+01	1.85e+02	3.35e+02	5.26e+02	5.85e+02	6.57e+02
8.00	0.45	2.88e+01	5.77e+01	1.07e+02	1.94e+02	2.97e+02	3.27e+02	3.61e+02
8.00	0.55	2.82e+00	1.23e+01	4.49e+01	1.58e+02	4.08e+02	5.07e+02	6.35e+02

Continued on next page

Table 3 – continued from previous page

E_{in}(MeV)	E_{out}(MeV)	N	Si	Fe	Ag	W	Pb	U
8.00	0.65	2.49e-02	5.57e-02	1.43e-01	6.96e-01	3.65e+00	5.52e+00	8.66e+00
8.00	0.75	4.40e-03	1.31e-02	5.57e-02	4.27e-01	2.57e+00	3.97e+00	6.37e+00
8.00	0.85	6.23e-04	4.49e-03	3.27e-02	3.03e-01	1.95e+00	3.02e+00	4.90e+00
8.00	0.95	4.90e-04	3.65e-03	2.52e-02	2.35e-01	1.51e+00	2.38e+00	3.86e+00
8.00	1.05	4.16e-04	3.00e-03	2.01e-02	1.83e-01	1.22e+00	1.90e+00	3.10e+00
8.00	1.15	3.54e-04	2.40e-03	1.65e-02	1.47e-01	9.67e-01	1.53e+00	2.51e+00
8.00	1.25	3.07e-04	2.03e-03	1.41e-02	1.21e-01	7.96e-01	1.25e+00	2.05e+00
8.00	1.35	2.72e-04	1.82e-03	1.16e-02	1.01e-01	6.63e-01	1.05e+00	1.72e+00
8.00	1.45	2.20e-04	1.54e-03	9.79e-03	8.34e-02	5.47e-01	8.72e-01	1.44e+00
8.00	1.55	1.91e-04	1.29e-03	8.46e-03	7.15e-02	4.68e-01	7.39e-01	1.22e+00
8.00	1.65	1.63e-04	1.21e-03	7.15e-03	6.06e-02	3.94e-01	6.30e-01	1.04e+00
8.00	1.75	1.37e-04	1.02e-03	6.49e-03	5.11e-02	3.35e-01	5.26e-01	8.92e-01
8.00	1.85	1.30e-04	9.36e-04	5.67e-03	4.50e-02	2.89e-01	4.64e-01	7.74e-01
8.00	1.95	1.15e-04	8.25e-04	5.40e-03	3.99e-02	2.54e-01	4.06e-01	6.78e-01
8.00	2.05	9.74e-05	7.25e-04	4.49e-03	3.51e-02	2.21e-01	3.55e-01	5.92e-01
8.00	2.15	9.05e-05	7.09e-04	4.09e-03	3.16e-02	1.98e-01	3.07e-01	5.15e-01
8.00	2.25	7.76e-05	6.42e-04	3.67e-03	2.83e-02	1.78e-01	2.80e-01	4.59e-01
8.00	2.35	7.03e-05	5.41e-04	3.40e-03	2.49e-02	1.54e-01	2.36e-01	4.00e-01
8.00	2.45	6.18e-05	5.20e-04	3.03e-03	2.20e-02	1.36e-01	2.17e-01	3.54e-01
8.00	2.55	5.50e-05	4.61e-04	2.71e-03	2.03e-02	1.20e-01	1.91e-01	3.14e-01
8.00	2.65	5.26e-05	4.27e-04	2.59e-03	1.82e-02	1.08e-01	1.70e-01	2.82e-01
8.00	2.75	4.78e-05	4.03e-04	2.29e-03	1.62e-02	9.74e-02	1.52e-01	2.49e-01
8.00	2.85	4.45e-05	3.40e-04	2.04e-03	1.39e-02	8.59e-02	1.35e-01	2.30e-01
8.00	2.95	3.68e-05	3.49e-04	1.85e-03	1.28e-02	7.68e-02	1.21e-01	2.02e-01
8.00	3.05	3.90e-05	2.95e-04	1.73e-03	1.22e-02	6.99e-02	1.10e-01	1.84e-01
8.00	3.15	3.51e-05	2.80e-04	1.53e-03	1.04e-02	6.19e-02	9.97e-02	1.63e-01
8.00	3.25	2.97e-05	2.34e-04	1.39e-03	9.62e-03	5.56e-02	8.92e-02	1.47e-01
8.00	3.35	3.11e-05	2.05e-04	1.11e-03	8.33e-03	5.18e-02	8.03e-02	1.35e-01
8.00	3.45	2.42e-05	1.90e-04	1.05e-03	7.63e-03	4.57e-02	7.28e-02	1.19e-01
8.00	3.55	2.51e-05	2.00e-04	1.01e-03	6.99e-03	4.07e-02	6.48e-02	1.09e-01
8.00	3.65	2.07e-05	1.45e-04	8.78e-04	6.11e-03	3.83e-02	5.83e-02	9.71e-02
8.00	3.75	1.95e-05	1.46e-04	7.69e-04	5.79e-03	3.31e-02	5.23e-02	8.64e-02
8.00	3.85	1.75e-05	1.20e-04	7.78e-04	4.95e-03	2.96e-02	4.69e-02	7.77e-02
8.00	3.95	1.67e-05	1.13e-04	6.91e-04	4.70e-03	2.64e-02	4.11e-02	7.02e-02
8.00	4.05	1.47e-05	1.04e-04	6.84e-04	3.92e-03	2.37e-02	3.85e-02	6.41e-02
8.00	4.15	1.61e-05	8.54e-05	5.44e-04	3.82e-03	2.10e-02	3.33e-02	5.66e-02
8.00	4.25	1.28e-05	8.84e-05	4.16e-04	3.43e-03	1.91e-02	3.03e-02	4.91e-02
8.00	4.35	1.26e-05	7.57e-05	4.00e-04	2.98e-03	1.76e-02	2.71e-02	4.52e-02
8.00	4.45	1.06e-05	6.92e-05	3.91e-04	2.60e-03	1.52e-02	2.53e-02	4.02e-02
8.00	4.55	1.06e-05	5.58e-05	3.33e-04	2.24e-03	1.29e-02	2.12e-02	3.65e-02
8.00	4.65	9.36e-06	5.34e-05	2.86e-04	2.04e-03	1.24e-02	1.83e-02	3.30e-02
8.00	4.75	8.06e-06	4.12e-05	2.62e-04	1.73e-03	1.02e-02	1.68e-02	2.88e-02
8.00	4.85	6.86e-06	3.81e-05	1.93e-04	1.52e-03	1.02e-02	1.55e-02	2.59e-02
8.00	4.95	5.66e-06	2.96e-05	2.40e-04	1.41e-03	8.64e-03	1.43e-02	2.36e-02
8.00	5.05	4.41e-06	3.78e-05	1.82e-04	1.30e-03	7.25e-03	1.25e-02	2.14e-02
8.00	5.15	4.23e-06	1.99e-05	1.53e-04	1.13e-03	6.44e-03	1.07e-02	1.77e-02
8.00	5.25	5.30e-06	2.30e-05	1.33e-04	1.05e-03	6.29e-03	9.63e-03	1.73e-02
8.00	5.35	3.36e-06	2.02e-05	1.16e-04	9.49e-04	5.42e-03	8.86e-03	1.44e-02

Continued on next page

Table 3 – continued from previous page

E_{in}(MeV)	E_{out}(MeV)	N	Si	Fe	Ag	W	Pb	U
8.00	5.45	3.09e-06	1.63e-05	1.11e-04	7.94e-04	4.61e-03	6.70e-03	1.31e-02
8.00	5.55	2.82e-06	2.41e-05	8.51e-05	6.79e-04	4.23e-03	6.77e-03	1.13e-02
8.00	5.65	2.73e-06	1.53e-05	9.03e-05	6.26e-04	3.17e-03	5.78e-03	1.03e-02
8.00	5.75	2.10e-06	1.02e-05	6.86e-05	5.48e-04	2.90e-03	5.05e-03	8.68e-03
8.00	5.85	2.17e-06	1.26e-05	5.53e-05	4.18e-04	2.88e-03	4.95e-03	8.56e-03
8.00	5.95	1.40e-06	5.79e-06	5.11e-05	4.13e-04	2.12e-03	4.11e-03	6.90e-03
8.00	6.05	1.17e-06	5.11e-06	2.55e-05	2.28e-04	2.12e-03	3.39e-03	5.71e-03
8.00	6.15	-	2.53e-06	1.99e-05	2.00e-04	1.66e-03	2.86e-03	5.07e-03
8.00	6.25	-	-	1.77e-05	2.24e-04	1.36e-03	2.44e-03	3.99e-03
8.00	6.35	-	-	1.39e-05	1.64e-04	1.17e-03	1.93e-03	3.58e-03
8.00	6.45	-	-	-	1.31e-04	1.11e-03	1.89e-03	3.32e-03
8.00	6.55	-	-	-	9.36e-05	1.01e-03	1.61e-03	2.68e-03
8.00	6.65	-	-	-	1.10e-04	7.23e-04	1.24e-03	2.51e-03
8.00	6.75	-	-	-	8.00e-05	7.38e-04	1.15e-03	2.21e-03
8.00	6.85	-	-	-	3.90e-05	5.58e-04	9.63e-04	1.94e-03
8.00	6.95	-	-	-	3.86e-05	3.79e-04	7.61e-04	1.45e-03
8.00	7.05	-	-	-	3.23e-05	3.75e-04	5.54e-04	1.25e-03
8.00	7.15	-	-	-	-	2.78e-04	5.64e-04	9.21e-04
8.00	7.25	-	-	-	-	2.06e-04	4.08e-04	7.59e-04
8.00	7.35	-	-	-	-	1.13e-04	2.17e-04	5.45e-04
8.00	7.45	-	-	-	-	1.64e-04	2.06e-04	3.89e-04
8.00	7.55	-	-	-	-	5.28e-05	1.34e-04	1.98e-04
8.00	7.65	-	-	-	-	-	8.21e-05	2.29e-04
8.00	7.75	-	-	-	-	-	6.30e-05	1.32e-04
8.00	7.85	-	-	-	-	-	-	7.55e-05

Table 4: Effective Photon Production Cross Sections (μb/sr·keV) for multi-MeV Photons Incident on Thick Targets (100 g/cm^2)

E_{in}(MeV)	E_{out}(MeV)	N	Si	Fe	Ag	W	Pb	U
2.00	0.15	1.03e+02	1.90e+02	1.80e+02	5.77e+01	2.22e+01	2.02e+01	5.62e+01
2.00	0.25	1.12e+02	2.25e+02	3.78e+02	3.63e+02	2.20e+02	1.97e+02	1.79e+02
2.00	0.35	3.34e+01	6.94e+01	1.31e+02	1.83e+02	1.53e+02	1.43e+02	1.35e+02
2.00	0.45	3.52e+00	8.88e+00	2.25e+01	5.20e+01	7.28e+01	7.48e+01	7.76e+01
2.00	0.55	3.06e+00	1.22e+01	4.38e+01	1.51e+02	3.56e+02	4.23e+02	5.04e+02
2.00	0.65	1.44e-02	8.86e-02	6.14e-01	3.61e+00	1.27e+01	1.69e+01	2.34e+01
2.00	0.75	2.67e-03	3.58e-02	3.35e-01	2.26e+00	9.04e+00	1.24e+01	1.82e+01
2.00	0.85	1.25e-03	2.08e-02	1.90e-01	1.40e+00	6.34e+00	8.87e+00	1.34e+01
2.00	0.95	5.51e-04	1.01e-02	1.10e-01	8.94e-01	4.46e+00	6.45e+00	1.02e+01
2.00	1.05	3.55e-04	5.80e-03	6.11e-02	5.49e-01	3.04e+00	4.51e+00	7.29e+00
2.00	1.15	1.90e-04	2.78e-03	3.25e-02	3.18e-01	2.01e+00	3.06e+00	5.13e+00
2.00	1.25	1.11e-04	1.47e-03	1.69e-02	1.77e-01	1.26e+00	2.00e+00	3.48e+00
2.00	1.35	6.11e-05	6.89e-04	8.10e-03	9.54e-02	7.59e-01	1.25e+00	2.22e+00
2.00	1.45	2.97e-05	4.12e-04	3.79e-03	4.62e-02	4.23e-01	7.18e-01	1.32e+00
2.00	1.55	2.40e-05	2.11e-04	1.85e-03	2.04e-02	2.17e-01	3.77e-01	7.48e-01
2.00	1.65	1.41e-05	1.26e-04	7.42e-04	8.33e-03	1.06e-01	1.85e-01	3.57e-01
2.00	1.75	2.96e-06	2.02e-05	1.43e-04	2.73e-03	4.11e-02	7.79e-02	1.52e-01
2.00	1.85	-	-	3.70e-05	1.08e-03	1.65e-02	2.95e-02	4.65e-02
2.00	1.95	-	-	2.26e-05	4.68e-04	3.20e-03	3.66e-03	8.22e-03
3.00	0.15	7.07e+01	1.42e+02	1.53e+02	5.99e+01	2.77e+01	2.54e+01	6.56e+01
3.00	0.25	7.09e+01	1.50e+02	2.75e+02	2.91e+02	1.85e+02	1.65e+02	1.49e+02
3.00	0.35	2.79e+01	6.18e+01	1.31e+02	2.15e+02	1.96e+02	1.82e+02	1.69e+02
3.00	0.45	5.62e+00	1.59e+01	4.52e+01	1.12e+02	1.48e+02	1.48e+02	1.43e+02
3.00	0.55	7.34e+00	2.95e+01	1.07e+02	3.58e+02	7.56e+02	8.58e+02	9.62e+02
3.00	0.65	5.14e-02	2.61e-01	1.58e+00	8.58e+00	2.72e+01	3.36e+01	4.31e+01
3.00	0.75	1.15e-02	1.25e-01	9.84e-01	5.88e+00	2.08e+01	2.67e+01	3.55e+01
3.00	0.85	5.47e-03	7.80e-02	6.54e-01	4.26e+00	1.62e+01	2.07e+01	2.85e+01
3.00	0.95	3.29e-03	5.08e-02	4.57e-01	3.10e+00	1.23e+01	1.64e+01	2.31e+01
3.00	1.05	2.16e-03	3.29e-02	3.21e-01	2.25e+00	9.52e+00	1.28e+01	1.84e+01
3.00	1.15	1.51e-03	2.13e-02	2.25e-01	1.66e+00	7.31e+00	1.01e+01	1.46e+01
3.00	1.25	9.91e-04	1.50e-02	1.59e-01	1.22e+00	5.65e+00	7.80e+00	1.15e+01
3.00	1.35	6.47e-04	9.98e-03	1.10e-01	8.89e-01	4.32e+00	5.99e+00	9.06e+00
3.00	1.45	4.07e-04	6.79e-03	7.77e-02	6.52e-01	3.28e+00	4.58e+00	7.02e+00
3.00	1.55	2.56e-04	4.79e-03	5.21e-02	4.63e-01	2.43e+00	3.53e+00	5.44e+00
3.00	1.65	1.58e-04	3.33e-03	3.79e-02	3.31e-01	1.86e+00	2.65e+00	4.16e+00
3.00	1.75	1.04e-04	2.42e-03	2.51e-02	2.32e-01	1.36e+00	1.98e+00	3.16e+00
3.00	1.85	7.65e-05	1.63e-03	1.80e-02	1.61e-01	9.83e-01	1.46e+00	2.36e+00
3.00	1.95	5.55e-05	1.32e-03	1.14e-02	1.12e-01	6.99e-01	1.05e+00	1.75e+00
3.00	2.05	3.99e-05	1.22e-03	8.42e-03	7.49e-02	4.85e-01	7.36e-01	1.27e+00
3.00	2.15	2.99e-05	8.82e-04	6.42e-03	5.01e-02	3.32e-01	5.16e-01	8.94e-01
3.00	2.25	2.57e-05	7.38e-04	4.29e-03	2.97e-02	2.15e-01	3.41e-01	5.99e-01
3.00	2.35	1.87e-05	5.69e-04	3.11e-03	2.03e-02	1.39e-01	2.14e-01	3.85e-01
3.00	2.45	1.39e-05	3.98e-04	2.22e-03	1.25e-02	8.56e-02	1.28e-01	2.30e-01
3.00	2.55	9.35e-06	1.97e-04	1.19e-03	7.29e-03	5.02e-02	7.88e-02	1.37e-01
3.00	2.65	5.25e-06	1.05e-04	6.70e-04	3.79e-03	2.31e-02	3.76e-02	7.08e-02
3.00	2.75	-	1.31e-05	1.01e-04	8.62e-04	1.10e-02	1.89e-02	3.39e-02

Continued on next page

Table 4 – continued from previous page

E_{in}(MeV)	E_{out}(MeV)	N	Si	Fe	Ag	W	Pb	U
3.00	2.85	-	-	-	4.24e-04	5.39e-03	1.00e-02	1.46e-02
3.00	2.95	-	-	-	2.15e-04	1.54e-03	1.42e-03	2.79e-03
4.00	0.15	5.69e+01	1.26e+02	1.54e+02	6.95e+01	3.50e+01	3.23e+01	8.04e+01
4.00	0.25	5.26e+01	1.19e+02	2.40e+02	2.81e+02	1.89e+02	1.69e+02	1.52e+02
4.00	0.35	2.35e+01	5.62e+01	1.32e+02	2.45e+02	2.37e+02	2.21e+02	2.03e+02
4.00	0.45	6.62e+00	2.04e+01	6.26e+01	1.64e+02	2.20e+02	2.15e+02	2.07e+02
4.00	0.55	1.05e+01	4.30e+01	1.59e+02	5.33e+02	1.09e+03	1.21e+03	1.33e+03
4.00	0.65	8.04e-02	4.22e-01	2.65e+00	1.48e+01	4.67e+01	5.69e+01	7.16e+01
4.00	0.75	2.09e-02	2.15e-01	1.75e+00	1.07e+01	3.73e+01	4.66e+01	6.05e+01
4.00	0.85	1.11e-02	1.41e-01	1.25e+00	8.00e+00	2.98e+01	3.81e+01	5.06e+01
4.00	0.95	7.28e-03	1.02e-01	9.12e-01	6.09e+00	2.40e+01	3.11e+01	4.23e+01
4.00	1.05	5.24e-03	7.25e-02	6.80e-01	4.73e+00	1.92e+01	2.53e+01	3.50e+01
4.00	1.15	3.76e-03	5.26e-02	5.16e-01	3.67e+00	1.55e+01	2.06e+01	2.88e+01
4.00	1.25	2.73e-03	3.93e-02	3.93e-01	2.87e+00	1.25e+01	1.66e+01	2.38e+01
4.00	1.35	1.99e-03	2.92e-02	2.98e-01	2.25e+00	9.96e+00	1.36e+01	1.94e+01
4.00	1.45	1.44e-03	2.18e-02	2.30e-01	1.76e+00	8.03e+00	1.09e+01	1.59e+01
4.00	1.55	1.01e-03	1.66e-02	1.76e-01	1.39e+00	6.48e+00	8.87e+00	1.29e+01
4.00	1.65	7.10e-04	1.23e-02	1.36e-01	1.08e+00	5.18e+00	7.10e+00	1.05e+01
4.00	1.75	4.93e-04	9.24e-03	1.04e-01	8.56e-01	4.11e+00	5.71e+00	8.50e+00
4.00	1.85	3.65e-04	7.71e-03	8.07e-02	6.63e-01	3.32e+00	4.58e+00	6.86e+00
4.00	1.95	2.37e-04	5.85e-03	6.15e-02	5.16e-01	2.63e+00	3.70e+00	5.60e+00
4.00	2.05	1.65e-04	4.94e-03	4.58e-02	4.02e-01	2.10e+00	2.89e+00	4.45e+00
4.00	2.15	1.25e-04	3.64e-03	3.54e-02	3.13e-01	1.65e+00	2.35e+00	3.60e+00
4.00	2.25	8.87e-05	3.12e-03	2.75e-02	2.37e-01	1.28e+00	1.83e+00	2.87e+00
4.00	2.35	6.89e-05	2.28e-03	2.12e-02	1.80e-01	1.02e+00	1.44e+00	2.28e+00
4.00	2.45	4.85e-05	1.68e-03	1.53e-02	1.31e-01	7.79e-01	1.13e+00	1.80e+00
4.00	2.55	3.47e-05	1.38e-03	1.14e-02	1.01e-01	5.83e-01	8.68e-01	1.41e+00
4.00	2.65	3.12e-05	9.93e-04	8.17e-03	7.17e-02	4.39e-01	6.45e-01	1.05e+00
4.00	2.75	2.34e-05	9.43e-04	6.67e-03	5.23e-02	3.36e-01	4.95e-01	8.16e-01
4.00	2.85	2.26e-05	6.63e-04	4.48e-03	3.88e-02	2.33e-01	3.63e-01	6.25e-01
4.00	2.95	1.87e-05	5.56e-04	3.29e-03	2.74e-02	1.82e-01	2.62e-01	4.51e-01
4.00	3.05	1.39e-05	3.90e-04	2.20e-03	1.94e-02	1.20e-01	1.87e-01	3.25e-01
4.00	3.15	9.94e-06	3.43e-04	1.95e-03	1.29e-02	8.40e-02	1.27e-01	2.25e-01
4.00	3.25	4.95e-06	2.12e-04	1.42e-03	8.10e-03	5.78e-02	8.42e-02	1.53e-01
4.00	3.35	2.47e-06	1.34e-04	6.73e-04	4.61e-03	3.56e-02	5.64e-02	1.00e-01
4.00	3.45	1.36e-06	8.80e-05	4.04e-04	2.61e-03	1.69e-02	3.12e-02	5.66e-02
4.00	3.55	7.39e-07	4.75e-05	2.74e-04	1.24e-03	8.95e-03	1.76e-02	3.03e-02
4.00	3.65	3.49e-07	1.58e-05	9.29e-05	6.28e-04	4.26e-03	7.09e-03	1.38e-02
4.00	3.75	5.10e-08	1.20e-06	2.39e-06	1.06e-04	1.68e-03	3.00e-03	5.65e-03
4.00	3.85	-	-	-	4.09e-05	7.18e-04	1.18e-03	1.68e-03
4.00	3.95	-	-	-	1.74e-05	1.13e-04	1.13e-04	2.83e-04
8.00	0.15	4.22e+01	1.25e+02	2.06e+02	1.20e+02	6.55e+01	6.07e+01	1.50e+02
8.00	0.25	3.04e+01	8.84e+01	2.42e+02	3.77e+02	2.85e+02	2.57e+02	2.31e+02
8.00	0.35	1.65e+01	5.07e+01	1.60e+02	3.89e+02	4.37e+02	4.16e+02	3.83e+02
8.00	0.45	8.13e+00	3.04e+01	1.11e+02	3.40e+02	5.01e+02	4.98e+02	4.78e+02
8.00	0.55	1.66e+01	7.26e+01	2.93e+02	1.06e+03	2.17e+03	2.38e+03	2.53e+03

Continued on next page

Table 4 – continued from previous page

E_{in}(MeV)	E_{out}(MeV)	N	Si	Fe	Ag	W	Pb	U
8.00	0.65	1.16e-01	8.44e-01	7.11e+00	4.88e+01	1.63e+02	1.97e+02	2.36e+02
8.00	0.75	4.43e-02	5.25e-01	5.09e+00	3.76e+01	1.38e+02	1.70e+02	2.11e+02
8.00	0.85	2.75e-02	3.76e-01	3.88e+00	2.98e+01	1.16e+02	1.46e+02	1.87e+02
8.00	0.95	1.93e-02	2.85e-01	3.06e+00	2.40e+01	9.78e+01	1.26e+02	1.64e+02
8.00	1.05	1.46e-02	2.19e-01	2.46e+00	1.98e+01	8.30e+01	1.08e+02	1.43e+02
8.00	1.15	1.14e-02	1.75e-01	1.98e+00	1.64e+01	7.09e+01	9.31e+01	1.25e+02
8.00	1.25	9.00e-03	1.39e-01	1.63e+00	1.38e+01	6.08e+01	7.99e+01	1.08e+02
8.00	1.35	7.19e-03	1.14e-01	1.34e+00	1.15e+01	5.20e+01	6.95e+01	9.41e+01
8.00	1.45	5.88e-03	9.42e-02	1.12e+00	9.79e+00	4.48e+01	5.93e+01	8.21e+01
8.00	1.55	4.70e-03	7.73e-02	9.48e-01	8.32e+00	3.87e+01	5.19e+01	7.18e+01
8.00	1.65	3.85e-03	6.42e-02	8.03e-01	7.09e+00	3.34e+01	4.45e+01	6.24e+01
8.00	1.75	3.13e-03	5.47e-02	6.67e-01	6.12e+00	2.90e+01	3.90e+01	5.44e+01
8.00	1.85	2.58e-03	4.62e-02	5.73e-01	5.26e+00	2.52e+01	3.39e+01	4.77e+01
8.00	1.95	2.18e-03	3.95e-02	4.89e-01	4.50e+00	2.19e+01	2.99e+01	4.17e+01
8.00	2.05	1.80e-03	3.28e-02	4.20e-01	3.87e+00	1.91e+01	2.56e+01	3.63e+01
8.00	2.15	1.42e-03	2.79e-02	3.53e-01	3.35e+00	1.66e+01	2.28e+01	3.22e+01
8.00	2.25	1.22e-03	2.42e-02	3.02e-01	2.94e+00	1.46e+01	1.97e+01	2.82e+01
8.00	2.35	1.02e-03	1.91e-02	2.66e-01	2.52e+00	1.27e+01	1.73e+01	2.47e+01
8.00	2.45	9.00e-04	1.73e-02	2.24e-01	2.17e+00	1.12e+01	1.53e+01	2.18e+01
8.00	2.55	7.58e-04	1.45e-02	1.99e-01	1.91e+00	9.65e+00	1.34e+01	1.93e+01
8.00	2.65	6.65e-04	1.25e-02	1.63e-01	1.65e+00	8.52e+00	1.20e+01	1.70e+01
8.00	2.75	5.38e-04	1.13e-02	1.48e-01	1.43e+00	7.41e+00	1.04e+01	1.49e+01
8.00	2.85	4.93e-04	9.38e-03	1.18e-01	1.25e+00	6.53e+00	9.06e+00	1.34e+01
8.00	2.95	4.19e-04	7.99e-03	1.08e-01	1.07e+00	5.74e+00	8.04e+00	1.19e+01
8.00	3.05	3.76e-04	6.92e-03	9.24e-02	9.17e-01	5.06e+00	6.96e+00	1.02e+01
8.00	3.15	3.36e-04	5.50e-03	7.66e-02	7.87e-01	4.34e+00	6.08e+00	9.09e+00
8.00	3.25	2.96e-04	5.15e-03	6.82e-02	6.92e-01	3.80e+00	5.32e+00	7.97e+00
8.00	3.35	2.52e-04	3.87e-03	5.60e-02	5.90e-01	3.38e+00	4.68e+00	6.93e+00
8.00	3.45	2.42e-04	3.76e-03	5.02e-02	5.26e-01	2.94e+00	4.07e+00	6.27e+00
8.00	3.55	2.23e-04	3.19e-03	3.96e-02	4.48e-01	2.52e+00	3.56e+00	5.48e+00
8.00	3.65	1.90e-04	2.43e-03	3.38e-02	3.79e-01	2.18e+00	3.10e+00	4.76e+00
8.00	3.75	1.61e-04	2.29e-03	3.14e-02	3.27e-01	1.89e+00	2.67e+00	4.14e+00
8.00	3.85	1.35e-04	2.01e-03	2.61e-02	2.59e-01	1.74e+00	2.39e+00	3.61e+00
8.00	3.95	1.19e-04	1.55e-03	2.12e-02	2.35e-01	1.39e+00	2.05e+00	3.17e+00
8.00	4.05	1.09e-04	1.61e-03	1.71e-02	1.99e-01	1.24e+00	1.76e+00	2.70e+00
8.00	4.15	9.45e-05	9.32e-04	1.55e-02	1.72e-01	1.05e+00	1.58e+00	2.40e+00
8.00	4.25	7.30e-05	7.62e-04	1.25e-02	1.42e-01	9.07e-01	1.30e+00	2.05e+00
8.00	4.35	7.36e-05	4.96e-04	9.92e-03	1.18e-01	7.49e-01	1.14e+00	1.76e+00
8.00	4.45	5.90e-05	5.98e-04	7.36e-03	9.57e-02	6.83e-01	9.20e-01	1.48e+00
8.00	4.55	5.07e-05	4.10e-04	5.56e-03	8.17e-02	5.81e-01	8.37e-01	1.26e+00
8.00	4.65	3.71e-05	3.36e-04	4.90e-03	6.50e-02	4.77e-01	6.93e-01	1.07e+00
8.00	4.75	4.20e-05	3.41e-04	3.76e-03	5.50e-02	3.97e-01	6.10e-01	9.79e-01
8.00	4.85	2.90e-05	2.76e-04	3.53e-03	4.63e-02	3.60e-01	4.94e-01	8.20e-01
8.00	4.95	2.26e-05	1.91e-04	2.71e-03	3.73e-02	2.91e-01	4.29e-01	6.97e-01
8.00	5.05	2.03e-05	1.86e-04	2.23e-03	2.95e-02	2.47e-01	3.54e-01	5.79e-01
8.00	5.15	1.71e-05	1.46e-04	1.82e-03	2.47e-02	1.93e-01	2.83e-01	5.18e-01
8.00	5.25	1.47e-05	1.09e-04	1.48e-03	2.02e-02	1.63e-01	2.43e-01	4.24e-01
8.00	5.35	1.21e-05	1.05e-04	1.20e-03	1.53e-02	1.37e-01	2.05e-01	3.48e-01

Continued on next page

Table 4 – continued from previous page

E_{in}(MeV)	E_{out}(MeV)	N	Si	Fe	Ag	W	Pb	U
8.00	5.45	1.03e-05	7.88e-05	9.37e-04	1.01e-02	1.11e-01	1.58e-01	3.07e-01
8.00	5.55	7.08e-06	7.23e-05	7.13e-04	1.02e-02	8.46e-02	1.53e-01	2.37e-01
8.00	5.65	6.30e-06	5.36e-05	6.00e-04	8.48e-03	6.92e-02	1.08e-01	1.87e-01
8.00	5.75	4.19e-06	3.68e-05	4.44e-04	4.63e-03	6.78e-02	8.97e-02	1.43e-01
8.00	5.85	3.51e-06	2.52e-05	3.66e-04	6.29e-03	5.00e-02	7.28e-02	1.28e-01
8.00	5.95	2.23e-06	2.29e-05	2.47e-04	4.29e-03	3.96e-02	6.34e-02	9.96e-02
8.00	6.05	1.37e-06	1.82e-05	1.88e-04	2.93e-03	3.01e-02	4.77e-02	8.61e-02
8.00	6.15	1.13e-06	7.14e-06	1.53e-04	2.03e-03	2.33e-02	3.81e-02	6.83e-02
8.00	6.25	-	1.00e-05	1.05e-04	1.75e-03	1.75e-02	2.75e-02	5.44e-02
8.00	6.35	-	3.63e-06	9.84e-05	1.33e-03	1.35e-02	2.22e-02	4.19e-02
8.00	6.45	-	-	4.97e-05	9.37e-04	1.02e-02	1.69e-02	3.14e-02
8.00	6.55	-	-	4.45e-05	6.08e-04	7.61e-03	1.30e-02	2.52e-02
8.00	6.65	-	-	3.26e-05	4.65e-04	5.47e-03	8.85e-03	1.89e-02
8.00	6.75	-	-	3.10e-05	3.38e-04	3.58e-03	6.65e-03	1.38e-02
8.00	6.85	-	-	1.40e-05	1.78e-04	2.87e-03	4.73e-03	9.52e-03
8.00	6.95	-	-	-	1.36e-04	1.88e-03	3.69e-03	7.76e-03
8.00	7.05	-	-	-	7.76e-05	1.24e-03	2.25e-03	4.80e-03
8.00	7.15	-	-	-	5.99e-05	7.55e-04	1.36e-03	3.20e-03
8.00	7.25	-	-	-	3.40e-05	4.92e-04	8.51e-04	2.02e-03
8.00	7.35	-	-	-	1.53e-05	2.78e-04	4.07e-04	1.00e-03
8.00	7.45	-	-	-	-	1.49e-04	2.05e-04	6.39e-04
8.00	7.55	-	-	-	-	6.24e-05	5.95e-05	2.81e-04
8.00	7.65	-	-	-	-	-	-	1.74e-04